ACS Catalysis

Research Article

pubs.acs.org/acscatalysis

Revealing the Dynamics of Platinum Nanoparticle Catalysts on Carbon in Oxygen and Water Using Environmental TEM

Langli Luo,[†] Mark H. Engelhard,[†] Yuyan Shao,*[,‡] and Chongmin Wang*[,†]

[†]Environmental Molecular Sciences Laboratory and [‡]Energy and Environment Directorate, Pacific Northwest National Laboratory, 902 Battelle Boulevard, Richland, Washington 99352, United States

Supporting Information

ABSTRACT: Deactivation of supported metal nanoparticle catalysts, especially under relevant gas conditions, is a critical challenge for many technological applications, including heterogeneous catalysis, electrocatalysis, and fuel cells. It has been commonly realized that deactivation of catalysts stems from surface area loss due to particle coarsening; however, the mechanism for this remains largely unclear. Herein, we use aberration-corrected environmental transmission electron microscopy, at an atomic level, to observe in situ the dynamics of Pt catalysts under fuel cell relevant gas and temperature conditions. Particle migration and coalescence is observed to be the dominant coarsening process. In comparison with the case of H_2O, O_2 promotes Pt nanoparticle migration on the carbon surface. Surprisingly, coating Pt/carbon with a nanofilm of electrolyte (Nafion ionomer) leads to a faster migration of Pt in H_2O than in O_2, a consequence of a Nafion−carbon interface water "lubrication" effect. Atomically, the particle coalescence features reorientation of particles toward lattice matching, a process driven by orientation-dependent van der Waals forces. These results provide direct observations of the dynamics of metal nanoparticles at the critical surface/interface under relevant conditions and yield significant insights into the multiphase interaction in related technological processes.

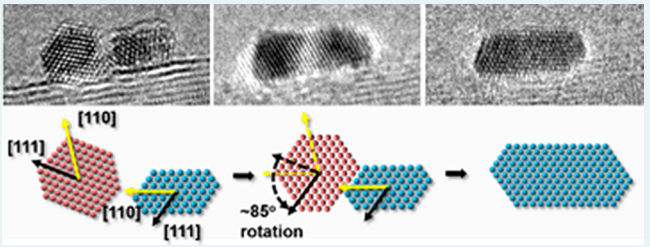

KEYWORDS: *platinum nanoparticle, environmental TEM, catalyst, atomic scale, water vapor, oxygen, in situ*

Platinum is one of the most widely used catalysts in many chemical and electrochemical reactions. A proton exchange membrane fuel cell (PEMFC) is considered to be an ideal power source for both stationary and mobile applications. The core component in a PEMFC is the membrane electrode assembly (MEA), in which a proton conducting ionomer membrane, usually Nafion, is sandwiched between two electrodes: the anode for the hydrogen oxidation reaction (HOR) and the cathode for the oxygen reduction reaction (ORR).[1] The two electrodes consist of Pt-based catalysts, Nafion ionomer (as binder and proton conductor), and gas diffusion layers. In comparison with the HOR at the anode, the ORR at the cathode, where molecular oxygen is reduced to form water, is not only the performance-limiting reaction in PEMFCs but also suffers from a rapid performance loss largely due to the deactivation of Pt nanoparticles.[2−5] Essentially, the durability of a Pt-based electrocatalyst determines the life cycle of the PEMFC and has been realized to be a prominent bottleneck for a broad application of PEMFCs, such as in fuel cell electrical vehicles (FCEV).[6] It has long been recognized that deactivation of the Pt-based electrocatalyst is directly related to the coarsening of the Pt nanoparticles under the working conditions of PEMFCs.[2,7,8] Extensive efforts have been made to stabilize the Pt nanoparticles on the support on an atomic scale, and strategies include alloying Pt with other elements,[9] encapsulating Pt nanoparticles,[10] enhancing the metal−support interaction through nanocomposites,[11] and combining physical and chemical stabilization.[12] However, the atomic scale fundamental coarsening mechanism and its correlation with the fuel cell operating gas conditions have never been fully understood.

Many techniques, such as X-ray absorption spectroscopy and transmission electron microscopy (TEM), have been used to study the durability of Pt electrocatalysts, usually by comparing the materials before and after the degradation test.[2,5,8,13,14] Such studies proved informative with respect to the possible degradation mechanisms of Pt electrocatalysts, but they are only limited to time-averaged static "images". Clearly, these traditional characterizations fall short in revealing the underlying dynamic process of the Pt catalysts and hence are unable to provide sufficient insights to guide the design of new electrocatalyst and operation protocols for better performance.

In situ TEM is a powerful tool to visualize the dynamic behavior of Pt nanoparticles and has been inherently used to reveal the possible deactivation mechanisms of the Pt nanoparticles.[15,16] Environmental TEM capable of simulating a gas environment at an elevated temperature provides an ideal platform for probing nanoscale/atomic scale materials properties in a relevant gas environment,[17] especially the dynamics of catalyst nanoparticles under controlled conditions, which has

Received: August 23, 2017
Revised: September 26, 2017
Published: September 29, 2017

DOI: 10.1021/acscatal.7b02861
ACS Catal. 2017, 7, 7658−7664

been proved to provide unprecedented insights for high-temperature heterogeneous catalysis,[18−20] but little has been reported on PEMFCs.[21−23] Herein, for the first time, we use an environmental TEM chamber with gases of O_2 and H_2O at 100 °C to simulate the working gas environment in PEMFCs as schematically illustrated in Figure 1, revealing atomic scale

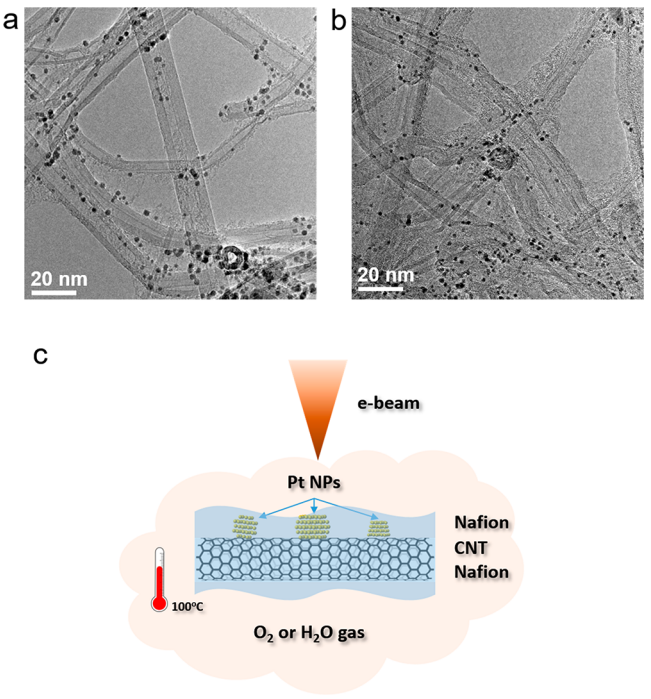

Figure 1. General morphologies of Pt/CNTs and Nafion/Pt/CNTs and experimental setup: (a) TEM image of Pt nanoparticles on CNTs; (b) TEM image of Nafion/Pt/CNTs; (c) schematic of in situ environmental TEM experimental setup showing the working conditions of Nafion/Pt/CNTs in O_2 or H_2O gases at 100 °C.

dynamics of Pt nanoparticles at the surface of carbon nanotubes and the Nafion−carbon interface. We found that particle migration and coalescence is the dominant coarsening mechanism. Surprisingly, we discovered that the migration rate of Pt nanoparticles sensitively depends on the gas environment and that the water-absorbing Nafion plays a critical role in the coarsening of Pt nanoparticles.

FASTER COARSENING OF Pt NANOPARTICLES IN O_2 THAN IN H_2O ON BARE CNTs

By monitoring the dynamic behavior of Pt nanoparticles supported on the CNT surface and exposed to O_2 and H_2O gas (0.01 mbar) at 100 °C, we found that the coarsening of Pt nanoparticles was dominated by the particle migration and coalescence process. Further, the migration and coalescence process is greatly promoted in O_2 gas in comparison with that in H_2O. In Figure 2, two series of time-lapse high-resolution (HR) TEM images depict the migration and coalescence process of Pt nanoparticles supported on CNTs. In O_2 (Figure 2a), atomically resolved images clearly show the dynamic migration of three couples of Pt nanoparticles (shown in white, black, and yellow dashed circles, respectively) in a period of 60 min. With the migration and coalescence of each pair of particles, it is always true that the smaller particle migrates toward the larger one, indicating a higher apparent migration barrier for large particles. Migration and coalescence of particles will lead to refaceting of the newly formed particle. The process of particle migration and coalescence proceeds at a much slower rate in H_2O than that in O_2 (Figure 2b), for which the particle migration and coalescences were not observed until 100 min and the merging of adjacent particles was seen after nearly 240 min. This observation clearly shows a faster migration rate of Pt nanoparticles on CNT surface in O_2 than that in H_2O gas environment. It is also noted that the CNTs show no obvious carbon erosion in both O_2 and H_2O, as confirmed by X-ray photoelectron spectroscopy (XPS) in Figure S2a in the Supporting Information.

We further revealed the atomistic process of the particle coalescence through in situ HRTEM imaging of two adjacent Pt nanoparticles and illustrated the promotion effect of O_2 for particle coalescence by switching the gas environment in situ from H_2O to O_2 while observing the dynamic behavior of the same pair of particles. To minimize the beam effect, a beam-blank experiment was employed so that the sample was only exposed to the beam to capture the HRTEM images, as shown in Figure 3. Two adjacent Pt nanoparticles with different

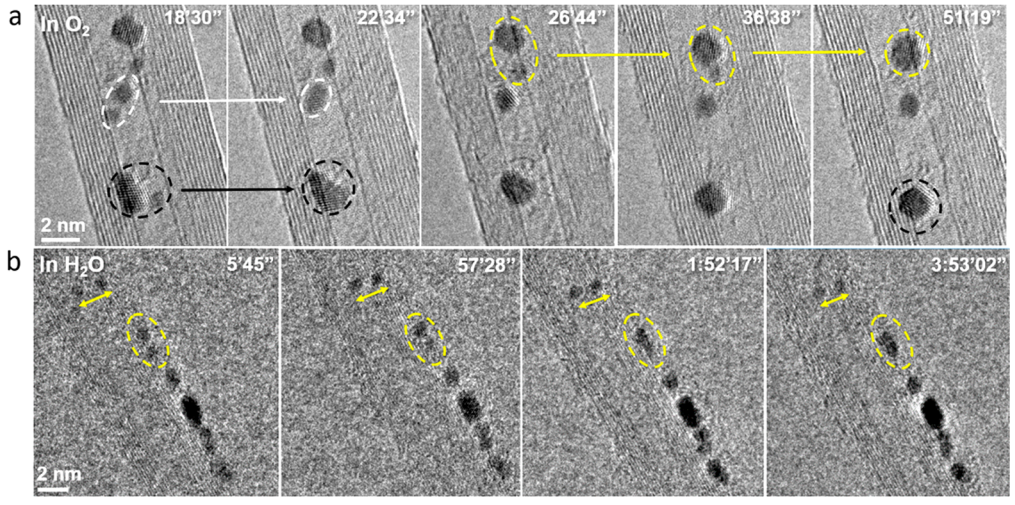

Figure 2. Coarsening process of Pt/CNTs in O_2 and H_2O gases at 100 °C: (a) in O_2 gas; (b) in H_2O gas (0.01 mbar). Two series of time-lapse HRTEM images reveal that the coarsening of Pt nanoparticles supported on CNTs is dominated by the migration and coalescence process.

DOI: 10.1021/acscatal.7b02861
ACS Catal. 2017, 7, 7658−7664

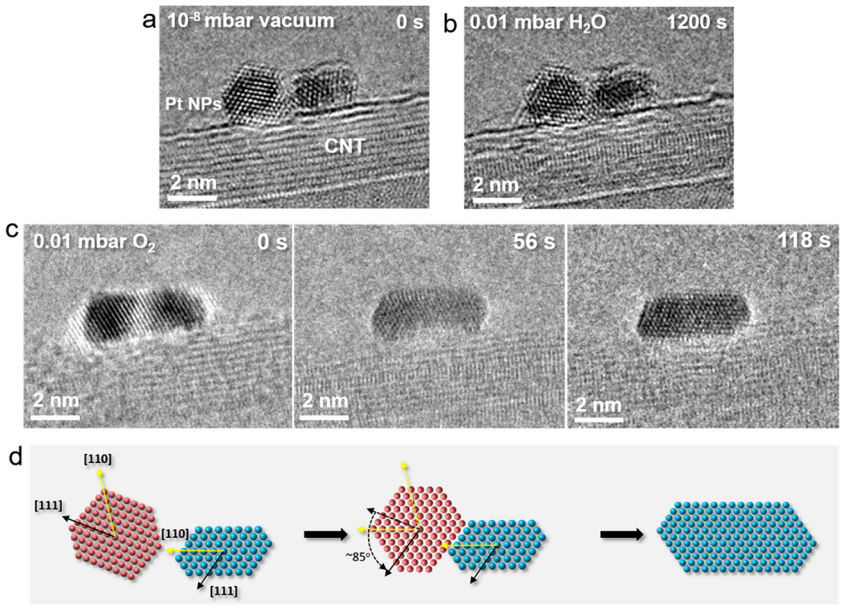

Figure 3. Migration and coalescence process of Pt/CNTs at 100 °C: (a) HRTEM image showing two separated Pt nanoparticles under vacuum; (b) HRTEM image showing that the distance between two Pt nanoparticles decreased but the nanoparticles still maintained their individual shape and orientation after 20 min in H_2O; (c) a series of time-lapsed HRTEM images showing the coalescence process of two Pt nanoparticles after switching the gas from H_2O to O_2; (d) schematic illustrating that the coalescence of these two Pt nanoparticles involves rotation of one NP and growth through orientation match.

surface facets were shown at a close distance but were separated in Figure 3a imaged under vacuum at 100 °C. After ~20 min in H_2O, the distance between these two particles slightly decreased, but they still maintained their surface facets, as evidenced in Figure 3b. After the gas was switched from H_2O to O_2, these two particles coalesced within 2 min to form a new particle with newly reconstructed surface facets, as shown in Figure 3c. Sequential images clearly revealed that the first step for coalescence is the rotation of the particle at the left side, as seen from the 0 s image, followed by the merging of the gap between these two nanoparticles, as seen in images of 56 s, and finally the formation of one larger single Pt NP, as shown in the image of 118 s. The newly formed Pt NP adopted the same orientation of the Pt NP at the right side, and the Pt NP at the left side went through a rotation of ~85°, as illustrated in Figure 3d, which is further confirmed by the HRTEM image simulation in Figure S2 in the Supporting Information.

The sequential steps of particle migration, orientation match, and coalescence observed in the gas environment as described above has never been reported previously but appears to be, phenomenologically, similar to the case of particle orientation attachment that was notably found in the solution growth of nanoparticles.[24,25] The underlying mechanism of particle orientation attachment in gas originates from the orientation-dependent van der Waals interaction between two particles, as theoretically predicted by Raju et al.[26] The present observation of particle migration on a support and coarsening through orientation attachment in a gas environment provides significant insights for exploring the deactivation mechanism of catalytic nanoparticles. It should be pointed out that the apparent migration barrier for an NP will depend on its size. The NP with a larger size always has a higher barrier for migration than that for a small NP. Hence, at 100 °C, some NPs with a relatively larger size are not observed to migrate.

The enhanced migration and coalescence of Pt nanoparticles on CNTs in O_2 gas, in comparison with that in H_2O, is associated with the strong Pt−O interaction. The interaction between Pt nanoparticles and the surface of CNTs is a weak van der Waals interaction.[27] DFT calculations have revealed that Pt nanoparticles only slightly wet on the graphite surface with an energy barrier for migration being in the magnitude of thermal energy.[28] On the other hand, oxygen chemisorption on Pt is known to be a thermodynamically favorable process, such that a surface oxide beyond a monolayer even can be formed with an O_2 pressure[29,30] of 0.01 mbar, as in the present experimental conditions. The formation of oxidized Pt is also confirmed by XPS analysis, as seen in Figure S2b in the Supporting Information. Since Pt nanoparticles are supported on the CNT surface, the O atoms would be expected to prefer to bond with Pt atoms in the perimeter through chemisorption or oxide growth to dewet the whole Pt NP,[31,32] facilitating the particle migration. Hence, both weak particle−substrate interactions and strong gas−particle interactions enhance the migration of Pt nanoparticles at an elevated temperature. In comparison with the Pt−O interaction, the Pt−H_2O interaction is much weaker, where H_2O is usually adsorbed intact as a molecule on the Pt surface without dissociation.[33] Hence, exposure to H_2O has the effect of less destabilization of Pt supported on CNT, and a slower migration rate of Pt nanoparticles on the CNT surface is expected in H_2O environment in accordance with the observation.

H_2O-PROMOTED Pt NANOPARTICLE MIGRATION AT NAFION/CNT INTERFACE

In a PEMFC, an ionomer electrolyte (Nafion) thin film covers the Pt/C catalysts in the electrode, leading to the Pt nanoparticles being spatially located at the interface between Nafion and carbon. In comparison with the case of Pt nanoparticles supported on CNT, covering Pt/CNT with a thin film of Nafion could potentially affect the Pt nanoparticle behavior during the operation of the PEMFC. Further, it is not clear how the Nafion evolves both structurally and chemically

DOI: 10.1021/acscatal.7b02861
ACS Catal. 2017, 7, 7658−7664

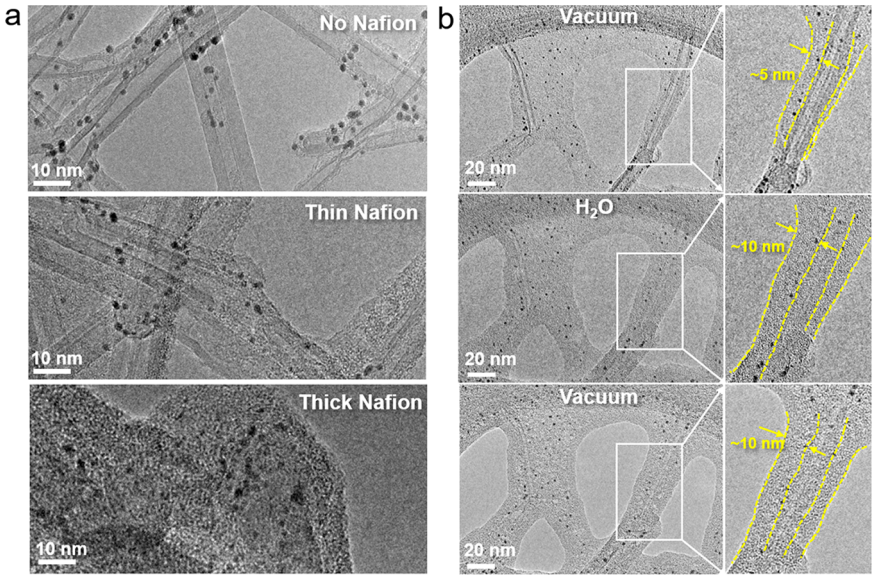

Figure 4. Morphologies of Nafion-coated Pt/CNTs and structural changes induced by H_2O absorption: (a) TEM images showing thin and thick Nafion layers coated on Pt/CNTs; (b) in situ TEM images showing the nonreversible expansion of the Nafion layer upon water introduction. Boxed enlarged areas show the thickness change of the Nafion layer from 5 nm (pristine under vacuum) to 10 nm (in H_2O), which remains 10 nm after removal of the H_2O gas.

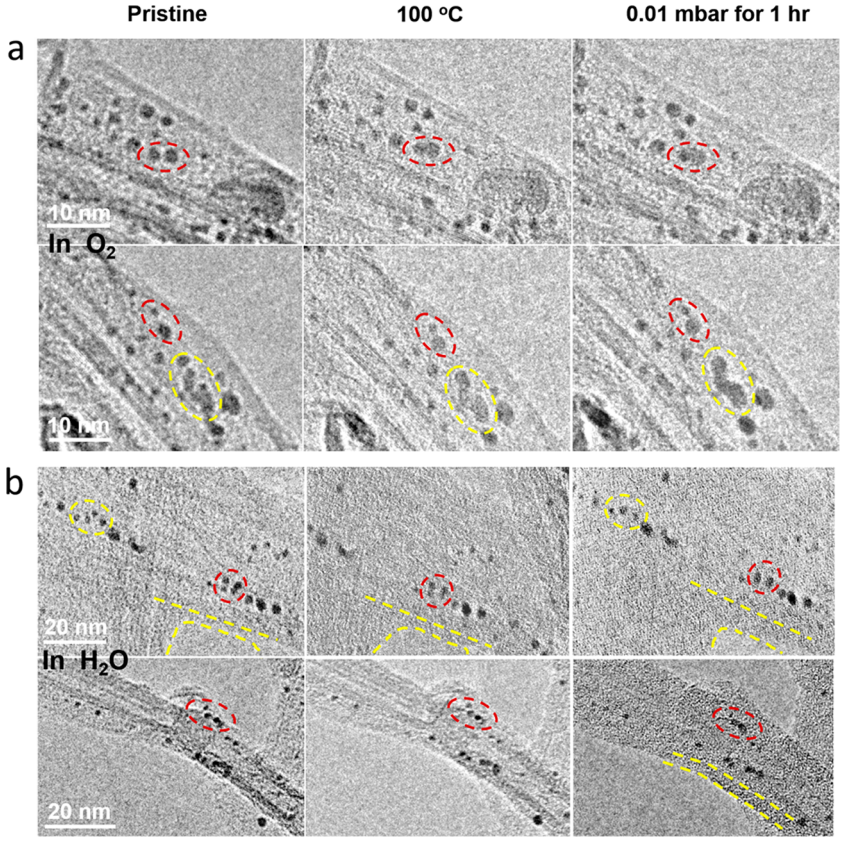

Figure 5. Coarsening process of Pt Nanoparticles at the interface of Nafion/carbon: TEM images showing the three statuses pristine (left column), 100 °C for 10 min (center column), and 100 °C for 1 h (right column) in gas of (a) O_2 and (b) H_2O. Dashed red and yellow circles keep track of the pertinent Pt nanoparticles for each case. In O_2 (a), most of the migration process of Pt nanoparticles happens during the thermal activation period (from left column to center column). In H_2O (b), Pt nanoparticles show significant migration and coalescence during the H_2O exposure period (from center column to right column). Enhanced coarsening in H_2O is shown at the Nafion/CNT interface. The yellow dashed lines in (b) illustrate the expansion of Nafion layers after introducing H_2O.

during the operation of the PEMFC. The general morphological features of the pristine Nafion-covered Pt/CNT catalysts is shown in Figure 4a. The thickness of Nafion films ranges from a few to tens of nanometers, and the coverage of the

DOI: 10.1021/acscatal.7b02861
ACS Catal. 2017, 7, 7658−7664

Nafion layer is more uniform for thicker Nafion layers. The Nafion films tended to spread and cover the surface of CNTs, indicating a good wetting of Nafion on the CNT surface. It is noted that, when a Nafion layer is cast onto the CNTs, the Pt nanoparticles were partially transferred from the CNT surface into the Nafion layer, as seen in Figure 4a, implying a weak Pt−CNT interaction.

The morphological evolution of Nafion/Pt/CNTs in H_2O at elevated temperature was directly monitored by using environmental TEM. The Nafion/Pt/CNT was exposed to H_2O vapor at 100 °C for 60 min. In comparison with the pristine structure, the Nafion film went through an expansion of ∼100% in H_2O, as indicated by yellow dashed lines in Figure 4b, a consequence of water-adsorption-induced Nafion polymer volume expansion. It would be expected that the H_2O-induced expansion of Nafion may also change the polymer molecular dynamics. Upon removal of H_2O, the Nafion film becomes porous, showing no noticeable shrinkage, as seen in the bottom image in Figure 4b. Generally, the thinner the Nafion film, the greater the expansion of the film upon exposure to H_2O, as shown in Figure S4 in the Supporting Information. Quantitative measurement indicates that the H_2O-induced expansion of Nafion films follows a gradual process and appears to show a self-limiting trend, as seen in the time-resolved images in Figure S5 in the Supporting Information. The morphological change of Nafion film in response to H_2O is believed to play a critical role in the mass transfer in a PEMFC.[34]

To evaluate the Pt nanoparticle coarsening characteristics in Nafion/Pt/CNTs and compare that with the case of Pt nanoparticles on CNT, the Nafion/Pt/CNTs were tested in situ in environmental TEM under the same conditions as those for Pt/CNTs shown in Figure 2. As seen in Figure 5, two series of TEM images were captured in O_2 and H_2O under three conditions: i.e., pristine, 100 °C, and 100 °C and 0.01 mbar of gas, respectively. In O_2, following 10 min at 100 °C, we do not notice significant migration and coalescence of Pt nanoparticles, as shown in Figure 5a. This is in apparent contrast with the behavior of Pt nanoparticles that are supported on CNTs without Nafion, indicating that the covering of Pt nanoparticles with Nafion inhibits the migration of Pt nanoparticles in O_2. In H_2O, Pt nanoparticles exhibit vigorous migration and coalescence, as evidenced by images shown in Figure 5b. It is noted that, only under the H_2O exposure, the Nafion layers show a noticeable expansion, as indicated by the yellow dashed lines in Figure 5b, indicating different structural modifications of Nafion upon exposure to O_2 and H_2O. These observations are in direct contrast to the coarsening behaviors of Pt nanoparticles on CNTs without Nafion layers, where the Pt nanoparticles were more prone to migrate and coalesce in O_2 in comparison to the case for H_2O, demonstrating that the Nafion layer plays a critical role in the coarsening process of Pt nanoparticles.

The results described above clearly indicate that the coarsening of Pt nanoparticles on CNTs with or without the Nafion layer proceeds via both a migration and a coalescence mechanism. In comparison with the case of vacuum, introduction of O_2 or H_2O in the system enhances the mobility of Pt nanoparticles. However, the effect of O_2 and H_2O on the migration rate of the Pt NP depends on the local environment of the Pt NP, as summarized in Figure 6. Pt nanoparticles supported on CNT shows a migration rate in O_2 much larger than that in H_2O, which is attributed to the weakened Pt−carbon interaction due to strong interaction

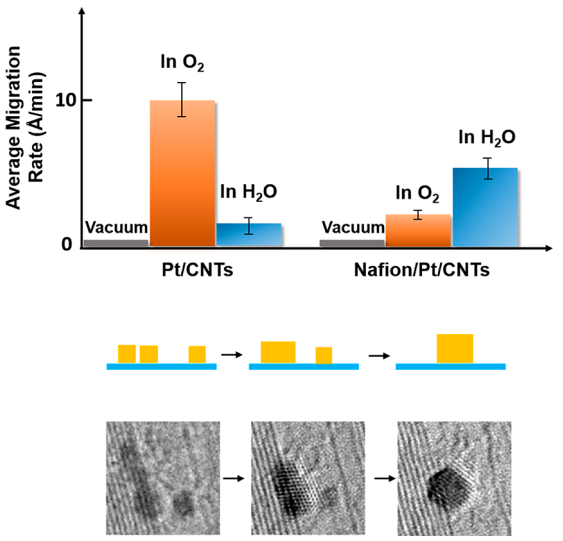

Figure 6. Summary of sintering mechanism and comparison of migration rates. The migration rates of Pt nanoparticles are compared between Pt/CNTs and Nafion/Pt/CNTs for different gas environments (vacuum, O_2, and H_2O). The schematic at the bottom illustrates that the sintering of Pt nanoparticles in both cases proceeds through a migration and coalescence process.

between O_2 and Pt nanoparticles. Covering of Pt/CNTs with Nafion leads to a reverse situation, where H_2O, in contrast to the case of O_2, was seen to boost the migration of Pt nanoparticles. This point is also supported by the change of the average size of the Pt NPs, as shown in Table S1 in the Supporting Information. It would be expected that, with the covering of the Pt nanoparticles on CNP by the Nafion, a prevailing mechanical confinement effect couples with the migration of the Pt nanoparticles. However, the distinctively different responses of Nafion to O_2 and H_2O lead to the variation of such a mechanical confinement effect with respect to Pt nanoparticle migration. Although Nafion is permeable to O_2, it has little effect on the mechanical confinement of the Nafion layer, where the migration of Pt nanoparticles is largely inhibited. In contrast, introduction of H_2O will lead to a large swelling of Nafion, which subsequently relieves the mechanical confinement effect for Pt NP migration. Moreover, the H_2O-soaked Nafion provides a highly humidified environment for Pt nanoparticles, where H_2O molecules likely "lubricate" both Pt−CNT and Pt−Nafion interfaces. It is the unique response of Nafion to H_2O that leads to an increased migration rate of Pt nanoparticles in comparison with that on a bare CNT surface.

The atomic-scale observation of nanoparticle migration and coalescence process shown in Figure 3 provides insights into the stability of Pt nanoparticles on the CNT surface. The high mobility of Pt NP originates from the weak interaction between CNT and Pt NP: i.e., the geometrical anchoring of Pt NP on CNT leads to a small contact area between Pt and the CNT surface, which subsequently facilitates nanoparticle migration and coalescence. Therefore, large contact area or enhancement of the Pt−carbon interface is essential for mitigating migration and coalescence and therefore prevents the deactivation of catalytic activity of the nanoparticles.

During the PEMFC operation, a range of factors will contribute to the coarsening of catalyst particles, typically those such as temperature, H_2O, O_2, electrochemical potential, and the interaction of Pt with Nafion and carbon nanotubes. It is

DOI: 10.1021/acscatal.7b02861
ACS Catal. 2017, 7, 7658−7664

known that Pt migration occurs at a high potential of over 0.8 V at 80 °C in PEMFC, while at room temperature, coarsening of Pt is strongly dependent on the Pt dissolution and redeposition.[35−38] For the present study, due to the challenge of building a fully functional PEMFC under the high vacuum of a TEM column, the in situ observations we have made are not fully based on a functioning PEMFC; rather what we captured in situ on the Pt coarsening by migration and coalescence only reflects the collective effect of temperature under the environment of O_2 and H_2O without external potential, for which Pt dissolution and electrochemical reaction are absent. Obviously, for a multifactor system, the effect of these factors on the Pt coarsening would not be a linear addition of the effect of each factor; the absence of the electrochemical conditions in the present case apparently will lead to the underestimation of the Pt coarsening rate in comparison with what happens under PEMFC operating conditions. Still, the significant difference observed in situ on the Pt coarsening rate under H_2O and O_2 provides insight into the fundamental understanding of how each of these factors contributes to the coarsening of the Pt nanoparticle. It should be noted that, in terms of physical and chemical properties, the commercially used active carbon in PEMFCs, especially for the case of functionalized carbon, is different from the CNT used in this study. However, what has been observed in this work reveals some fundamental processes as to how O_2 and H_2O affect the interaction of the Pt NP with carbon, therefore providing insight into how to mitigate the Pt NP coarsening process, such as through surface functionalization. Apparently, more work needs to be done to use the carbon support that is tailored for a PEMFC system.

In summary, direct in situ TEM observation reveals unprecedented details at the atomic scale with respect to the behavior of Pt nanoparticles for fuel cell applications, especially the coarsening dynamics of Pt nanoparticles on a bare CNT surface and in Nafion-covered Pt/CNTs in an O_2 and H_2O gas environment. We found that the coarsening of Pt nanoparticles proceeded through a migration and coalescence process. The migration rate of Pt nanoparticles on a bare CNT surface is much faster in O_2 than that in H_2O. The strong oxygen chemisorption on Pt nanoparticles weakens the interaction between Pt and the CNT surface, leading to a fast migration in O_2. Incorporation of a Nafion electrolyte layer creates a mechanical confinement to Pt/CNTs, which reduces the Pt migration rate in O_2. However, this mechanical confinement is largely relieved by introducing H_2O, and a lubricated interface is created, both leading to a faster migration rate of Pt in H_2O than that in O_2. These results bridge the gap between the previous in situ TEM studies under idealized conditions and the technologically relevant conditions of Pt catalysts for PEMFCs, thus providing insights into the rational design of Pt/carbon catalysts incorporating Nafion electrolyte to achieve long-lasting PEM fuel cells.

METHODS

Preparation of Pt/CNTs/Nafion. Pt/CNT was prepared by the ethylene glycol (EG) reduction method, as detailed in our previous publications.[39,40] Typically, 2.656 mL of hexachloroplatinic acid (H_2PtCl_6) EG solution (7.53 mg Pt mL−1 EG) was mixed with 50 mL of EG solution. A 1.0 M NaOH solution (in EG) was used to adjust the pH of the solution to >13. An 80 mg portion of CNT was added to the above solution, and the mixture was stirred for 60 min and subsequently heated under reflux conditions at 130 °C for 4 h. After the mixture was cooled and stirred for an additional 12 h, nitric acid solution was added to adjust the solution to a pH of 2. The resulting catalyst was washed with warm ultrapure DI water and then dried at 90 °C under vacuum for 3 h. The as-synthesized Pt/CNTs were suspended in methanol and drop-casted on lacey-carbon Cu TEM grids. The Nafion solution (5 wt %) was diluted (1:20) and drop-casted on the Cu grids to coat the Pt/CNTs to form Nafion-covered Pt/CNTs.

Environmental TEM Studies. Environmental TEM (FEI Titan ETEM) is equipped with an objective-lens aberration corrector enabling sub-Angstrom HRTEM imaging. A customized gas delivery system enabled precise pressure control from the base pressure ~2×10^{-8} mbar to 10 mbar. A customized water vapor delivery system introduced H_2O gas into the ETEM with a purity of >96% and up to a pressure of 0.1 mbar. The system is composed of a diaphragm pump, a vacuum gauge, and a water reservoir. The diaphragm pump creates a vacuum to let the water vapor fill in the pipeline, and when the pumping−filling process is repeated, a high purity of water vapor can be achieved. The Pt/CNTs or Nafion/Pt/CNTs loaded on TEM grids were mounted on a Gatan double-tilt heating holder (Model 652) and inserted into the TEM column. The sample was first brought up to 100 °C and then quickly exposed to the ambient gas of O_2, H_2, and H_2O with a partial pressure of ~0.01 mbar. On the basis of our calibration of the effect of the electron beam,[41] we chose a beam dose rate of 300 electron/(Å^2 s) and took one image every 5 or 10 min for a total time span of 1−4 h, leading to a typical cumulative beam dose of 7.2×10^3 to 1.44×10^4 electron/Å^2 with 1 s exposure for each image, which is far below the limit of the safe zone.

HRTEM Image Simulation. To confirm the HRTEM contrast of the dynamics of Pt nanoparticles on CNTs, we used the atomic structure models of Pt nanoparticles generated by CrystalMaker through Wulff construction as an input to calculate the HRTEM images and compared the simulated image with the experimentally captured image. The HRTEM image simulation of the Pt NP was carried out using the multislicing method with SimulaTEM code.[42] The parameters for the image simulation were chosen as follows: accelerating voltage of 300 kV and spherical aberration coefficient of the objective lens of 2 μm.

Measurements of Migration Rates. The migration rates were measured through chosen Pt nanoparticles with a sample size of tens of nanoparticles over a time period of up to 4 h. The rates were averaged for each experimental condition.

ASSOCIATED CONTENT

Supporting Information

The Supporting Information is available free of charge on the ACS Publications website at DOI: 10.1021/acscatal.7b02861.

Additional information and Figures S1−S6 and Table S1 as described in the text (PDF)

AUTHOR INFORMATION

Corresponding Authors

*E-mail for Y.S.: Yuyan.shao@pnnl.gov.

*E-mail for C.W.: Chongmin.wang@pnnl.gov.

ORCID

Langli Luo: 0000-0002-6311-051X

Chongmin Wang: 0000-0003-3327-0958

DOI: 10.1021/acscatal.7b02861
ACS Catal. 2017, 7, 7658−7664

Notes

The authors declare no competing financial interest.

■ ACKNOWLEDGMENTS

This work was supported by the Laboratory Directed Research and Development Program at Pacific Northwest National Laboratory (PNNL). The work was conducted in the William R. Wiley Environmental Molecular Sciences Laboratory (EMSL), a national scientific user facility sponsored by DOE's Office of Biological and Environmental Research and located at PNNL. PNNL is operated by Battelle for the DOE under Contract DE-AC05-76RLO1830.

■ REFERENCES

(1) Gasteiger, H. A.; Kocha, S. S.; Sompalli, B.; Wagner, F. T. *Appl. Catal., B* **2005**, *56*, 9−35.
(2) Ferreira, P. J.; la O', G. J.; Shao-Horn, Y.; Morgan, D.; Makharia, R.; Kocha, S.; Gasteiger, H. A. *J. Electrochem. Soc.* **2005**, *152*, A2256−A2271.
(3) Shao, Y.; Yin, G.; Gao, Y. *J. Power Sources* **2007**, *171*, 558−566.
(4) Borup, R.; Meyers, J.; Pivovar, B.; Kim, Y. S.; Mukundan, R.; Garland, N.; Myers, D.; Wilson, M.; Garzon, F.; Wood, D.; Zelenay, P.; More, K.; Stroh, K.; Zawodzinski, T.; Boncella, J.; McGrath, J. E.; Inaba, M.; Miyatake, K.; Hori, M.; Ota, K.; Ogumi, Z.; Miyata, S.; Nishikata, A.; Siroma, Z.; Uchimoto, Y.; Yasuda, K.; Kimijima, K.-i.; Iwashita, N. *Chem. Rev.* **2007**, *107*, 3904−3951.
(5) Arenz, M.; Zana, A. *Nano Energy* **2016**, *29*, 299−313.
(6) Shrestha, S.; Liu, Y.; Mustain, W. E. *Catal. Rev.: Sci. Eng.* **2011**, *53*, 256−336.
(7) Wilson, M. S.; Garzon, F. H.; Sickafus, K. E.; Gottesfeld, S. *J. Electrochem. Soc.* **1993**, *140*, 2872−2877.
(8) Shao, Y.; Yin, G.; Gao, Y.; Shi, P. *J. Electrochem. Soc.* **2006**, *153*, A1093−A1097.
(9) Lu, N.; Wang, J.; Xie, S.; Xia, Y.; Kim, M. J. *Chem. Commun.* **2013**, *49*, 11806−11808.
(10) Cheng, N.; Banis, M. N.; Liu, J.; Riese, A.; Li, X.; Li, R.; Ye, S.; Knights, S.; Sun, X. *Adv. Mater.* **2015**, *27*, 277−281.
(11) Cheng, N.; Norouzi Banis, M.; Liu, J.; Riese, A.; Mu, S.; Li, R.; Sham, T.-K.; Sun, X. *Energy Environ. Sci.* **2015**, *8*, 1450−1455.
(12) Im, J.; Choi, M. *ACS Catal.* **2016**, *6*, 2819−2826.
(13) Yano, H.; Watanabe, M.; Iiyama, A.; Uchida, H. *Nano Energy* **2016**, *29*, 323−333.
(14) Mezzavilla, S.; Cherevko, S.; Baldizzone, C.; Pizzutilo, E.; Polymeros, G.; Mayrhofer, K. J. J. *ChemElectroChem* **2016**, *3*, 1524−1536.
(15) Simonsen, S. B.; Chorkendorff, I.; Dahl, S.; Skoglundh, M.; Sehested, J.; Helveg, S. *J. Am. Chem. Soc.* **2010**, *132*, 7968−7975.
(16) Challa, S. R.; Delariva, A. T.; Hansen, T. W.; Helveg, S.; Sehested, J.; Hansen, P. L.; Garzon, F.; Datye, A. K. *J. Am. Chem. Soc.* **2011**, *133*, 20672−20675.
(17) Zhang, X.; He, Y.; Sushko, M. L.; Liu, J.; Luo, L.; De Yoreo, J. J.; Mao, S. X.; Wang, C.; Rosso, K. M. *Science* **2017**, *356*, 434−437.
(18) Hansen, P. L.; Wagner, J. B.; Helveg, S.; Rostrup-Nielsen, J. R.; Clausen, B. S.; Topsøe, H. *Science* **2002**, *295*, 2053−2055.
(19) DeLaRiva, A. T.; Hansen, T. W.; Challa, S. R.; Datye, A. K. *J. Catal.* **2013**, *308*, 291−305.
(20) Hansen, T. W.; DeLaRiva, A. T.; Challa, S. R.; Datye, A. K. *Acc. Chem. Res.* **2013**, *46*, 1720−1730.
(21) Benavidez, A. D.; Kovarik, L.; Genc, A.; Agrawal, N.; Larsson, E. M.; Hansen, T. W.; Karim, A. M.; Datye, A. K. *ACS Catal.* **2012**, *2*, 2349−2356.
(22) Yoshida, K.; Xudong, Z.; Bright, A. N.; Saitoh, K.; Tanaka, N. *Nanotechnology* **2013**, *24*, 065705.
(23) Yoshida, K.; Bright, A. N.; Ward, M. R.; Lari, L.; Zhang, X.; Hiroyama, T.; Boyes, E. D.; Gai, P. L. *Nanotechnology* **2014**, *25*, 425702.
(24) Li, D.; Nielsen, M. H.; Lee, J. R. I.; Frandsen, C.; Banfield, J. F.; De Yoreo, J. J. *Science* **2012**, *336*, 1014−1018.
(25) De Yoreo, J. *Nat. Mater.* **2013**, *12*, 284−285.
(26) Raju, M.; van Duin, A. C. T.; Fichthorn, K. A. *Nano Lett.* **2014**, *14*, 1836−1842.
(27) Henderson, M. A. *Surf. Sci. Rep.* **2002**, *46*, 1−308.
(28) Ramos-Sanchez, G.; Balbuena, P. B. *Phys. Chem. Chem. Phys.* **2013**, *15*, 11950−11959.
(29) Krasnikov, S. A.; Murphy, S.; Berdunov, N.; McCoy, A. P.; Radican, K.; Shvets, I. V. *Nanotechnology* **2010**, *21*, 335301.
(30) Miller, D. J.; Öberg, H.; Kaya, S.; Sanchez Casalongue, H.; Friebel, D.; Anniyev, T.; Ogasawara, H.; Bluhm, H.; Pettersson, L. G. M.; Nilsson, A. *Phys. Rev. Lett.* **2011**, *107*, 195502.
(31) Ackermann, M. D.; Pedersen, T. M.; Hendriksen, B. L. M.; Robach, O.; Bobaru, S. C.; Popa, I.; Quiros, C.; Kim, H.; Hammer, B.; Ferrer, S.; Frenken, J. W. M. *Phys. Rev. Lett.* **2005**, *95*, 255505.
(32) Getman, R. B.; Xu, Y.; Schneider, W. F. *J. Phys. Chem. C* **2008**, *112*, 9559−9572.
(33) Ogasawara, H.; Brena, B.; Nordlund, D.; Nyberg, M.; Pelmenschikov, A.; Pettersson, L. G. M.; Nilsson, A. *Phys. Rev. Lett.* **2002**, *89*, 276102.
(34) Weber, A. Z.; Borup, R. L.; Darling, R. M.; Das, P. K.; Dursch, T. J.; Gu, W.; Harvey, D.; Kusoglu, A.; Litster, S.; Mench, M. M.; Mukundan, R.; Owejan, J. P.; Pharoah, J. G.; Secanell, M.; Zenyuk, I. V. *J. Electrochem. Soc.* **2014**, *161*, F1254−F1299.
(35) Bi, W.; Gray, G. E.; Fuller, T. F. *Electrochem. Solid-State Lett.* **2007**, *10*, B101−B104.
(36) Dubau, L.; Castanheira, L.; Berthomé, G.; Maillard, F. *Electrochim. Acta* **2013**, *110*, 273−281.
(37) Nikkuni, F. R.; Vion-Dury, B.; Dubau, L.; Maillard, F.; Ticianelli, E. A.; Chatenet, M. *Appl. Catal., B* **2014**, *156-157*, 301−306.
(38) Arán-Ais, R. M.; Yu, Y.; Hovden, R.; Solla-Gullón, J.; Herrero, E.; Feliu, J. M.; Abruña, H. D. *J. Am. Chem. Soc.* **2015**, *137*, 14992−14998.
(39) Shao, Y.; Zhang, S.; Kou, R.; Wang, X.; Wang, C.; Dai, S.; Viswanathan, V.; Liu, J.; Wang, Y.; Lin, Y. *J. Power Sources* **2010**, *195*, 1805−1811.
(40) Shao, Y.; Zhang, S.; Wang, C.; Nie, Z.; Liu, J.; Wang, Y.; Lin, Y. *J. Power Sources* **2010**, *195*, 4600−4605.
(41) Wu, J.; Helveg, S.; Ullmann, S.; Peng, Z.; Bell, A. T. *J. Catal.* **2016**, *338*, 295−304.
(42) Gómez-Rodríguez, A.; Beltrán-del-Río, L. M.; Herrera-Becerra, R. *Ultramicroscopy* **2010**, *110*, 95−104.

DOI: 10.1021/acscatal.7b02861
ACS Catal. 2017, 7, 7658−7664